JCI The Journal of Clinical Investigation

Neutrophil-mediated innate immune resistance to bacterial pneumonia is dependent on Tet2 function

Candice Quin, … , Michael J. Rauh, Dawn M.E. Bowdish

J Clin Invest. 2024. https://doi.org/10.1172/JCI171002.

Research In-Press Preview **Immunology** **Infectious disease**

Individuals with clonal hematopoiesis of indeterminate potential (CHIP) are at increased risk of aging related health conditions and all-cause mortality, but whether CHIP impacts risk of infection is much less clear. Using UK Biobank data, we revealed a positive association between CHIP and incident pneumonia in 438,421 individuals. We show that inflammation enhanced pneumonia risk, as CHIP carriers with a hypomorphic IL6 receptor polymorphism were protected. To better characterize the pathways of susceptibility, we challenged hematopoietic *Tet Methylcytosine Dioxygenase 2* knockout (*Tet2*$^{-/-}$) and floxed control mice (*Tet2*$^{f/f}$) with *Streptococcus pneumoniae*. As with human CHIP carriers, *Tet2*$^{-/-}$ mice had hematopoietic abnormalities resulting in the expansion of inflammatory monocytes and neutrophils in peripheral blood. Yet, these cells were insufficient in defending against *S. pneumoniae* and resulted in increased pathology, impaired bacterial clearance, and higher mortality in *Tet2*$^{-/-}$ mice. We delineated the transcriptional landscape of *Tet2*$^{-/-}$ neutrophils and found that while inflammation-related pathways were upregulated in *Tet2*$^{-/-}$ neutrophils, migration and motility pathways were compromised. Using live-imaging techniques, we demonstrated impairments in motility, pathogen uptake and neutrophil extracellular trap (NET) formation by *Tet2*$^{-/-}$ neutrophils. Collectively, we show that CHIP is a risk factor for bacterial pneumonia related to innate immune impairments.

Neutrophil-mediated innate immune resistance to bacterial pneumonia is dependent on Tet2 function

Candice Quin,[1,2,8] Erica N. DeJong,[1,2] Elina K. Cook,[3] Yi Zhen Luo,[3] Caitlyn Vlasschaert,[3] Sanathan Sadh,[3] Amy J.M. McNaughton,[3] Marco Buttigieg,[3] Jessica A. Breznik,[1,2] Allison E. Kennedy,[1,2] Kevin Zhao,[1,2] Jeffrey Mewburn,[6] Kimberly J. Dunham-Snary,[4,6] Charles Hindmarch,[5,6] Alexander G. Bick,[7] Stephen L. Archer,[5,6] Michael J. Rauh,[3] & Dawn M.E. Bowdish[1,2§]

[1] Department of Medicine, Faculty of Health Sciences, McMaster University, ON, Canada

[2] Firestone Institute for Respiratory Health, St. Joseph's Healthcare Hamilton, ON, Canada

[3] Department of Pathology and Molecular Medicine, Faculty of Health Sciences, Queen's University, ON, Canada

[4] Department of Biomedical and Molecular Sciences, Queen's University, Canada

[5] Queen's CardioPulmonary Unit, Queen's University, Canada

[6] Department of Medicine, Queen's University, Canada

[7] Division of Genetic Medicine, Department of Medicine, Vanderbilt University Medical Center, Nashville, TN, USA

[8] Institute of Medical Sciences, School of Medicine, Medical Sciences and Nutrition, University of Aberdeen, United Kingdom

§Corresponding author Dawn M.E. Bowdish, McMaster University Michael DeGroote Centre for Learning & Discovery, 1-905-525-9140 ext. 22313, bowdish@mcmastser.ca

The authors have declared that no conflict of interest exists

ABSTRACT

Individuals with clonal hematopoiesis of indeterminate potential (CHIP) are at increased risk of aging related health conditions and all-cause mortality, but whether CHIP impacts risk of infection is much less clear. Using UK Biobank data, we revealed a positive association between CHIP and incident pneumonia in 438,421 individuals. We show that inflammation enhanced pneumonia risk, as CHIP carriers with a hypomorphic IL6 receptor polymorphism were protected. To better characterize the pathways of susceptibility, we challenged hematopoietic *Tet Methylcytosine Dioxygenase 2* knockout (*Tet2*$^{-/-}$) and floxed control mice (*Tet2*$^{f/f}$) with *Streptococcus pneumoniae*. As with human CHIP carriers, *Tet2*$^{-/-}$ mice had hematopoietic abnormalities resulting in the expansion of inflammatory monocytes and neutrophils in peripheral blood. Yet, these cells were insufficient in defending against *S. pneumoniae* and resulted in increased pathology, impaired bacterial clearance, and higher mortality in *Tet2*$^{-/-}$ mice. We delineated the transcriptional landscape of *Tet2*$^{-/-}$ neutrophils and found that while inflammation-related pathways were upregulated in *Tet2*$^{-/-}$ neutrophils, migration and motility pathways were compromised. Using live-imaging techniques, we demonstrated impairments in motility, pathogen uptake and neutrophil extracellular trap (NET) formation by *Tet2*$^{-/-}$ neutrophils. Collectively, we show that CHIP is a risk factor for bacterial pneumonia related to innate immune impairments.

INTRODUCTION

Human aging is accompanied by dysregulation of hematopoiesis in the bone marrow (BM), which may have adverse clinical consequences (1). Hematopoiesis is a tightly regulated process by which hematopoietic stem cells (HSC) differentiate into functional and mature blood cells. As HSCs reside and cycle in the BM, they naturally acquire mutations that are then passed on to their progeny, resulting in clonal hematopoiesis. Acquired mutations that are advantageous to cell survival accumulate over time (2). When the resultant mutant clones and their variant alleles are found at a frequency of ≥2% in peripheral blood cell DNA, this is defined as clonal hematopoiesis of indeterminate potential (CHIP) (3). The occurrence of CHIP increases with age and it is estimated that 10-20% of adults aged 65 and above are CHIP carriers (4). By contrast, somatic CHIP clones are detectable in less than 1% of individuals under the age of 40 (5). The mutational events that drive CHIP occur most frequently in the *DNA Methyltransferase 3 Alpha* (*DNMT3A*), and *Tet Methylcytosine Dioxygenase 2* (*TET2*) genes (6). Although these genes have seemingly opposing enzymatic roles on DNA methylation, *DNMT3A* methylating versus *TET2* demethylating (7), many studies have demonstrated convergent effects of mutations in these genes on inflammatory and hematopoietic pathways. For instance, both *TET2* and *DNMT3A* inactivating mutations appear to have important roles in dysregulating the differentiation and function of myeloid cells, like monocytes and neutrophils. Both human and murine studies have shown that loss-of-function in either *TET2* (8-10) or *DNMT3A* (11) biases hematopoiesis towards the myeloid lineage, which ultimately results in an imbalanced ratio of myeloid/lymphoid cells, termed myeloid skewing. Monocytes isolated from mutant-*DNMT3A* carriers have increased expression of pro-inflammatory genes compared to those without *DNMT3A* mutations (12). This includes genes encoding inflammatory mediators such as interleukin (IL)6 and IL8, chemokine (C-C motif)

ligands 4 (CCL4) and resistin, which promotes monocyte adhesion to endothelial cells (12, 13). Several studies have also supported a role for mutant-*TET2* clones in promoting macrophage inflammation and the secretion of pro-inflammatory mediators, including IL6 (14-16). It has been suggested that aberrant inflammation from CHIP myeloid clones may underpin various comorbid diseases such as hematopoietic cancers and cardiovascular disease (17, 18), including pulmonary arterial hypertension (19). More recently, a relationship between clonal hematopoiesis and risk of severe infections, including various lung infections, has been identified (20) but the mechanisms and pathways of susceptibility are not known.

Lower respiratory tract infections such as pneumonia are among the most common cause of infectious disease related hospitalizations and are a leading cause of morbidity and mortality worldwide (21). Older adults are at a higher risk of developing pneumonia and having more adverse outcomes (22). This increased risk is thought to be driven by an age-related remodeling of the immune system (1). With increasing age, HSCs committed to the myeloid lineage outnumber those committed to the lymphoid lineage in both humans and mice, resulting in myeloid skewing (23). This phenomenon is accompanied by age-related changes in myeloid cell subsets that favour inflammation. For instance, circulating $Ly6C^{high}$ inflammatory monocytes increase with age in mice and express more of the chemokine receptor, CCR2 (24). These monocytes, which are equivalent to $CD14^{+}CD16^{-}$ classical and $CD14^{+}CD16^{++}$ inflammatory monocytes in humans (25), produce higher levels of pro-inflammatory cytokines than their $Ly6C^{low}$/non-classical counterparts, and as a result, are often associated with immunopathology (24, 26). Moreover, in humans, having higher than age-average levels of inflammatory cytokines in circulation increases the risk of developing pneumonia and other age-related diseases (27). Although the link between age-associated inflammation and poor clinical outcomes to respiratory infections has a robust

epidemiological basis, it lacks conclusive mechanistic explanations (28). We and others (20, 29) postulate that clonal hematopoiesis, which connects aging, aberrant myelopoiesis, and inflammation, may explain this phenomenon.

To determine whether CHIP has a disease-modifying role in pneumonia, we leveraged data from the UK Biobank to establish a relationship between CHIP and incident pneumonia. We then challenged *Tet2* hematopoietic knockout (*Tet2*$^{-/-}$) and floxed control mice (*Tet2*$^{f/f}$) with *Streptococcus pneumoniae* to better characterize the pathways of susceptibility in mutant-*TET2* CHIP. The research presented here suggests that naturally occurring mutations in *TET2* are a major risk factor for bacterial pneumonia, driven by myeloid immune cell dysfunction. Critically, this work highlights dysfunctional *Tet2*-mutant neutrophils as pivotal cells in *S. pneumoniae* pathogenesis, and a possible target for therapeutic intervention in CHIP carriers.

RESULTS

CHIP is a risk factor for bacterial pneumonia

We sought to determine the role of CHIP in pneumococcal disease risk using data from the UK Biobank. The cohort included 438,421 individuals, of whom 14,787 (3.3%) had CHIP clones detected at variant allele fraction (VAF) ≥2%. In agreement with previous reports (30), mutations in *TET2* and *DNMT3A* were the most frequently identified mutated genes associated with CHIP. We demonstrate that risk of pneumonia events was increased in individuals with CHIP (Figure 1A). CHIP carriers had a 1.23-fold higher risk of incident pneumonia than non-carriers after correcting for age, sex, and other covariates. These epidemiological data indicate that there is a significant association between CHIP carrier status and incidence of pneumonia.

Previous reports have demonstrated that inflammatory mediators such as IL6 increase CHIP-comorbid risk to cardiovascular disease (31). To determine if inflammation influenced the risk of incident pneumonia in CHIP carriers, we added an interaction term for a common single nucleotide polymorphism (SNP) in the IL6 receptor gene (*IL6R* [rs2228415]) that reduces IL6 signaling. We show that a heightened risk of *Streptococcus pneumoniae* pneumonia in CHIP (Figure 1A) carriers that was abrogated in individuals with this hypomorphic IL6R SNP (in those with low genetic IL6R). These results indicate that a lower inflammatory status may be beneficial for reducing pneumonia risk in CHIP carriers.

CHIP contributes to myeloid expansion

Abnormal peripheral blood neutrophil and monocyte numbers may increase pneumonia risk (32). Using flow cytometry, we examined peripheral blood leukocytes in 22 participants from the

greater Hamilton area in Canada with or without CHIP at steady-state, ascertained using our previously-described 48-gene targeted CHIP panel (33). The characteristics of the study population are displayed in Supplemental Table 1**.** The participants ranged from 56 to 100 years of age and consisted of 14 females (63.6%) and 8 males. There were no significant differences in body mass index (BMI) or sex distribution among participants. Of the CHIP carriers (n=6), 50% had mutant-*DNMT3A* clones and 50% had mutant-*TET2* clones detected as variant allele fraction (VAF) ≥2%. We found that innate immune cell numbers varied significantly with CHIP carrier status such that CHIP carriers had higher numbers of total monocytes, classical monocytes and neutrophils (Figure 1, B-D) in whole blood, consistent with myeloid expansion. No differences in absolute and relative numbers of intermediate and non-classical monocytes were observed. We found that the CHIP carriers had lower levels of the chemokines CXCL1 and CXCL5 in serum, which are important for neutrophil recruitment and mobilization in response to lung infections (Figure 1, E and F). CHIP carriers also expressed lower levels of the high-affinity Fc-gamma receptor, CD64, on circulating neutrophils (Figure 1G). Taken together, these data provide evidence that alterations in myeloid cell populations in CHIP carriers may increase risk of bacterial pneumonia.

Tet2 mutations increase innate immune cell numbers and inflammation in circulation

To better characterize the pathways of susceptibility, we employed mice with *Tet2*-knockout directed to the hematopoietic system (*Vav1-iCre*$^{+}$*;Tet2*$^{-/-}$, i.e. *Tet2*$^{-/-}$) and control (*Vav1-iCre-;Tet2*$^{f/f}$, i.e. *Tet2*$^{f/f}$) mice. As with human CHIP carriers, the *Tet2*$^{-/-}$ mice had hematopoietic abnormalities at steady-state, resulting in the expansion of both the number and relative proportion (as a percentage of CD45^{+} leukocytes) of monocytes in peripheral blood (Figure 2A). Though not

significant, there was also a tendency for blood neutrophil counts to increase (Figure 2B). Murine monocytes can be divided into subsets by their surface expression of the glycoprotein Ly6C into $Ly6C^{low}$ and $Ly6C^{high}$ monocytes (34, 35). Monocytes expressing high levels of Ly6C have pro-inflammatory functions and tend to express low levels of CX3C chemokine receptor 1 (CX_3CR_1) (25). Accordingly, we found that the proportion of $Ly6C^{high}$ monocytes was higher in *Tet2*$^{-/-}$ mice, whilst the proportion expressing low CX_3CR_1 was decreased (Figure 2, C and D). Consistent with their ascribed function, we demonstrated that these monocytes were more inflammatory and produced higher levels of tumor necrosis factor alpha (TNF) in response to LPS stimulation (Figure 2E). Subsequent analyses using a multiplexed-ELISA for key pro-inflammatory cytokines (TNF, IL6, and IL1β) re-affirmed the exacerbated TNF response in the serum of *Tet2*$^{-/-}$ mice following stimulation with LPS (Figure 2F). Additionally, we found an increased IL6 response in *Tet2*$^{-/-}$ mice as compared to *Tet2*$^{f/f}$ mice (Figure 2G) and a significant induction of IL1β that was not observed in the *Tet2*$^{f/f}$ mice following LPS stimulation (Figure 3H). Taken together, these data demonstrate that changes in monocyte subsets may contribute to excessive inflammation in *Tet2*$^{-/-}$ mice during bacterial challenge.

Tet2 regulates expansion and emigration of myeloid cell lineages

To determine whether *Tet2*-related changes in monocyte numbers, phenotype and inflammatory capacity were related to changes in myelopoiesis, we examined hematopoietic stem and progenitor (HSPC) cell populations in the BM. In agreement with previous reports (8), we found that *Tet2* loss-of-function increased HSPC proliferation, giving rise to an increase in myeloid-biased multipotent progenitor cells. We found that the proportion of common myeloid progenitors (CMP), monocyte-dendritic progenitors (MDP), granulocyte-monocyte progenitors (GMPs) and common

monocyte progenitors (cMoP) all increased in *Tet2*$^{-/-}$ mice (Figure 3, A-E). Since progenitor numbers were similar between the groups, we sought to determine if an increase in monocyte emigration in *Tet2*$^{-/-}$ mice could account for differences in circulating myeloid populations. The C-C chemokine receptor type 2 (CCR2) is required for leukocytes, and especially Ly6C^{high} monocytes to leave the BM and enter the blood (36). As such, we hypothesized that enhanced CCR2 expression could prompt their emigration from the BM and could further explain their increased number seen in the circulation of *Tet2*$^{-/-}$ mice. In support of this notion, we demonstrated a significant increase in Ly6C^{high} CCR2 expression in the BM of *Tet2*$^{-/-}$ mice (Figure 3F). Thus, mobilization of inflammatory monocytes to the blood may be increased in *Tet2*$^{-/-}$ mice.

We have previously shown that *Tet2*-deficient BM progenitors have a proliferative advantage in the presence of TNF (37). Based on this, we explored whether differences in bone marrow TNF responsiveness exists between *Tet2*$^{-/-}$ and *Tet2*$^{f/f}$ mice. We found, as in the peripheral blood, that inflammatory Ly6C^{high} monocytes in BM express higher TNF following stimulation with LPS (Figure 3G). Not only was TNF increased, but also the expression of the TNF receptor CD120b (TNFR2) (Figure 3H). Taken together, these data suggest that an inflammatory environment may propagate the expansion of *TET2*-mutant myeloid cells, contributing to clonal dominance.

Tet2$^{-/-}$ *mice exhibit a pathological myeloid response to S. pneumoniae*

To determine the clinical relevance of myeloid expansion in CHIP carriers, we challenged *Tet2*$^{-/-}$ and *Tet2*$^{f/f}$ mice with *Streptococcus pneumoniae*. Consistent with previous reports in wildtype C57Bl/6 mice, the number of *Tet2*$^{f/f}$ mice that became moribund and required euthanasia always did so between days 2 and 4 post-infection (p.i.), at the peak of symptom activity. Mice that survived past day 4 p.i. recovered from the infection. In contrast, morbidity and mortality were

prolonged in the *Tet2*$^{-/-}$ mice, whose health continued to decline 7 days after *S. pneumoniae* colonization (Figure 4A), resulting in higher overall mortality (64% in *Tet2*$^{-/-}$ mice versus 18% in *Tet2*$^{f/f}$ mice). At 10 days post infection, the surviving *Tet2*$^{-/-}$ mice exhibited severe lung pathology including large areas of necrosis and hemorrhage, marked thickening of the bronchial mucosa and widespread inflammatory cell infiltration into the alveoli (Figure 4, B and C), as compared to the floxed control mice (*Tet2*$^{f/f}$).

Investigation of differential cellular influx in the lungs of *Tet2*$^{-/-}$ mice revealed an increase in mononuclear phagocytes (F4/80^{+} macrophages, monocytes, and dendritic cells) (Figure 4D), when compared to *Tet2*$^{f/f}$ mice. In contrast, we found that neutrophils (Ly6G^{+}) were decreased in the lungs of *Tet2*$^{-/-}$ mice. Evaluation of the peripheral blood likewise showed increases in the relative number of monocytes in the *Tet2*$^{-/-}$ mice; however surprisingly, the proportion of peripheral blood neutrophils were also higher in *Tet2*$^{-/-}$ mice (Figure 4E). We postulated that neutrophil recruitment to the lungs may be impaired in *Tet2*$^{-/-}$ mice. In order to test whether neutrophils had an intrinsic migration defect we injected CCL2 (MCP-1) into the intraperitoneal cavity. We found no differences between *Tet2*$^{-/-}$ and *Tet2*$^{f/f}$ mice (Supplemental Figure 1), suggesting no inherent defects in trans-endothelial migration. We next investigated whether lower recruitment of neutrophils in the lung might be a consequence of defective chemotactic signaling. In support of this, we found that CCL2 expression was decreased in the lungs and surface CCR2 expression was decreased on peripheral blood neutrophils in *Tet2*$^{-/-}$ mice, at steady-state (Figure 4, F and G). Taken together, these results indicate that *Tet2* deficiency confers an inappropriate and pathological myeloid cell response in pneumonia.

Tet2$^{-/-}$ *mice have impaired clearance of S. pneumoniae*

To determine whether the reduced neutrophil recruitment in *Tet2*$^{-/-}$ mice altered pathogen load, we quantified CFUs from multiple organs at critical and experimental endpoint. At critical endpoint, the numbers of *S. pneumoniae* recovered from the complete nasal turbinates (CNT), lungs, spleens and brain of the *Tet2*$^{-/-}$ mice were similar to the numbers recovered from the *Tet2*$^{f/f}$ mice (Supplemental Figure 2). In both groups, a large number of *S. pneumoniae* could be recovered from multiple organs, highlighting the severity of disease in these animals. In contrast, the pathogen burden at experimental endpoint (day 10 p.i.) was significantly different between *Tet2*$^{-/-}$ and *Tet2*$^{f/f}$ mice. The *Tet2*$^{-/-}$ mice which survived to day 10 p.i. had higher counts of *S. pneumoniae* in the CNT, as compared to the *Tet2*$^{f/f}$ mice (Figure 4H**)**. A similar trend was observed in the lungs, although this did not reach statistical significance. These data suggest that *Tet2*$^{-/-}$ mice are less successful at clearing *S. pneumoniae*, despite the increased number of mononuclear phagocytes.

To address if the impaired clearance of *S. pneumoniae* in *Tet2*$^{-/-}$ mice was accompanied by excessive or unregulated inflammation that is typical of sepsis (38), we correlated the main inflammatory mediators *TNF, IL6, IFNγ, MCP1*, and *IL1β* in circulation with corresponding CFUs in the CNT at day 10 p.i.. There was a significant positive relationship between CFUs and all inflammatory mediators in the CNT (Figure 4I). Similar results were observed in the lungs (Supplemental Figure 3). This data provides evidence that an exaggerated inflammatory response accompanies reduced bacterial clearance.

Tet2$^{-/-}$ *neutrophils have impaired motility, phagocytosis and NET formation*

Next, we sought to determine if differences in CFUs reflect impaired uptake or removal of pathogen by *Tet2*$^{-/-}$ phagocytes. To test this, we examined the killing capacity of BM-derived macrophages (BMDM) isolated from *Tet2*$^{-/-}$ and *Tet2*$^{f/f}$ mice. No differences were observed in *S.*

pneumoniae killing between the groups (Figure 5A). To determine whether the observed CFUs could instead be due to neutrophil impairments, we measured neutrophil binding and uptake. Despite similar bacterial binding capabilities, we observed reduced or delayed bacterial internalization in *Tet2*$^{-/-}$ neutrophils (Figure 5B), resulting in impaired killing of *S. pneumoniae* (Figure 5C). Using complimentary live imaging techniques, we found that compared to *Tet2*$^{f/f}$, *Tet2*$^{-/-}$ neutrophils phagocytosed fewer bacteria (*S. aureus*) (Figure 5, D and E) and moved more slowly, covering less distance (Figure 5, F-H). We also found that *Tet2*$^{-/-}$ neutrophil extracellular trap (NET) formation in response to *S. aureus*, was impaired (Figure 5, I and J). The *Tet2*$^{f/f}$ neutrophils formed large NETs whereas the *Tet2*$^{-/-}$ neutrophils were smaller in surface area with fewer spindle-like projections. Based on prior findings (39), we postulated that differences in neutrophil maturity might be responsible for reducing neutrophil phagocytic capacity and antimicrobial function. In keeping with this hypothesis, we found that *Tet2*$^{-/-}$ mice had higher numbers of immature neutrophils ($CD11b^{+}Ly6G^{+}CD101^{-}$) in circulation (Figure 5K). Overall, *Tet2*-deficient murine neutrophils have compromised immune functions.

Impaired motility and migratory gene pathways in Tet2$^{-/-}$ *neutrophils*

To further explore the mechanisms of *Tet2*$^{-/-}$ neutrophil dysfunction, we examined changes in gene expression using whole transcriptome sequencing (RNA-seq). In total, we identified 130 genes which were differentially abundant in the *Tet2*$^{-/-}$ versus *Tet2*$^{f/f}$ control neutrophils. Specific pathways highlighted in *Tet2*$^{-/-}$ neutrophils demonstrate a clear pro-inflammatory signature, with enrichment of 40 genes involved in immunity and defense pathways (Figure 6). Strikingly, the remaining 99 genes were significantly downregulated *Tet2*$^{-/-}$ neutrophils. These *Tet2*$^{-/-}$-specific genes were determined to be central in motility and migratory pathways. Taken together, these

molecular data provide evidence that *Tet2*$^{-/-}$ neutrophils mediate a paradoxical state of enhanced inflammation but also reduced phagocytic capacity, which has clinical consequences during infection.

DISCUSSION

There is emerging evidence that individuals with clonal hematopoiesis are at increased risk of severe infections (20), but the mechanisms and pathways of susceptibility are not known. Consistent with previous reports (17), we show that murine hematopoietic *Tet2*-knockout and *TET2*-mutant CHIP promotes changes in the hematopoietic system in both mice and humans, resulting in dysregulated myelopoiesis. In mice, the proportion of BM HSCs committed to the myeloid lineage were consistently higher in *Tet2*$^{-/-}$ animals compared to control. This was accompanied by an increase in CCR2 expression, which promotes the release of monocytes into circulation (36). We showed that in both mice and humans, inflammatory subsets of monocytes (Ly6C^{high} and classical monocytes, respectively) increased with *Tet2/TET2*-inactivation. In addition, we demonstrate that like *Dnmt3a*-mutant cells (40), myeloid cells from *Tet2*$^{-/-}$ mice have a greater proclivity to become hyper-activated in response to inflammatory insults, such as TNF, resulting in increased production of inflammatory cytokines and myeloid expansion. We postulate that the increased response could be mediated through increased TNFR2 expression, (40) although this remains to be formally demonstrated. Taken together, these data support the notion that defects in *Tet2* promote a hyper-inflammatory immunogenic profile, that may contribute to worse outcomes of infections (20) and other CHIP comorbid conditions (41).

Clearance of a pneumococcal pneumonia requires an appropriate innate immune response, particularly by phagocytic cells such as neutrophils and monocytes. Despite the importance of these myeloid lineage cells in controlling pathogen burden, an exacerbated inflammatory response can cause lung damage and pathology, and may become the primary source of morbidity and mortality (42). Impairment of innate resolution in the lungs has been linked to poorer outcomes in several models of bacterial and viral pulmonary infections (43-45). Thus, successful control of

pneumococcal infections requires not only neutrophil and monocyte clearance of the invading pathogens, but also resolution of these immune cells to prevent tissue damage. Here, we show that *Tet2*$^{-/-}$ mice have a pronounced increase in pulmonary monocytes following infection, which failed to resolve by day 10 p.i. We show that the persistence of these highly inflammatory cells resulted in lung damage without effective pathogen clearance.

The inability of *Tet2*$^{-/-}$ mice to effectively clear *S. pneumoniae* was attributed to impaired neutrophil function. Our results show that CC chemokine receptors and their ligands, which are necessary for neutrophil mobilization and recruitment to the lungs during infection (46-48), are down-regulated in human CHIP carriers (e.g. CXCL1, CXCL5) and mice (e.g. CCR2, lung CCL2). As we did not see any differences in neutrophil trans-endothelial migration towards an administered chemoattractant, we attribute the reduced numbers of neutrophils in the lungs to reduced chemotactic signalling, rather than inherent defects in recruitment. It is also possible that the neutrophils were more efficiently cleared from the lungs by the increased presence of monocytes, but additional studies are needed to fully address this question. Nevertheless, in humans with CHIP we also found decreased expression of CD64, an Fc receptor associated with neutrophil activation and phagocytosis. Previous studies have demonstrated that a worse prognosis and survival in patients correlated with decreased expression of CD64 and with impaired neutrophil phagocytic activity (49). The authors proposed that neutrophil phagocytic activity may serve as a prognostic indicator of sepsis. Excessive immature forms of neutrophils are also related to clinical deterioration in patients with sepsis (39). Consistent with these findings, we show that *Tet2*$^{-/-}$ mice had an increase in immature neutrophils in peripheral blood and that the neutrophils isolated from *Tet2*$^{-/-}$ mice had reduced or delayed bacterial phagocytic activity and cell motility. We also show that the expulsion of neutrophil nuclear contents to form NETs was impaired in

Tet2$^{-/-}$ neutrophils *ex vivo*, which may be due to reduced CXCL1-CXCR2 signaling (47). Further characterization of *Tet2*$^{-/-}$ neutrophils using RNA-sequencing revealed that gene pathways important for phagocytic functions (i.e. motility) were reduced, rendering *Tet2*$^{-/-}$ mice highly susceptible to *S. pneumoniae*. Overall, we demonstrate that *Tet2* mutations drive known sepsis features, such as cytokine driven hyperinflammatory response and immunosuppression, characterized by reduced activity of phagocytes (50). These findings broaden our understanding of the role of Tet enzymes in regulating infectious disease outcomes and highlight innate immune dysfunction as a key contributor to pneumonia risk in mutant-*TET2* CHIP carriers.

MATERIALS AND METHODS

Sex as a biological variable

Our study examined male and female animals, and similar findings are reported for both sexes.

UK Biobank cohort

The UK Biobank is a large observational cohort of individuals residing in the United Kingdom, which contains baseline demographic information such as age, sex, and health habits as well as ongoing clinical health records. From this dataset, we determined the CHIP status for all participants with available whole exome data (n=453,510), as detailed previously (51). Individuals with a history of hematologic cancer at enrollment are excluded from the CHIP dataset Incident pneumonia was defined using the UKB field IDs 131446 through 131457, which correspond to the dates of first report of pneumonia (ICD-10 codes J13-J18) from any source (death register, primary care, hospital admissions, or self-report).

Human subjects and CHIP genotyping

Community dwelling research participants were recruited from the Greater Hamilton Area (Ontario, Canada) between November 2017 and January 2020. Venous blood was drawn in anti-coagulant-free vacutainers for the isolation of serum, and in heparin-coated vacutainers for the experiments that required viable leukocytes.(52) Participant demographic information (age, sex, height) and health status (components of the Charlson Comorbidity Index [CCI], body mass index [BMI], medication history, vaccination history, and frailty scores) were provided at the time of sample collection. Only participants who had not required antibiotics within two weeks of sample

collection were included in this analysis. CHIP status was determined by applying a successful 48-gene, targeted, Ion-Torrent based sequencing approach to isolated genomic DNA from peripheral blood mononuclear cells with a VAF ≥2%, as previously described (33, 51).

Animals

Tet2$^{f/f}$ (B6;129S-Tet2tm1.1Iaai/J) and *Vav1-iCre* (B6.Cg-Tg(Vav1-icre)A2Kio/J) mice were bred at Queen's University to produce *Tet2*$^{f/f}$ *Vav1-icre*$^{-/-}$ (*Tet2*$^{f/f}$) and *Tet2*$^{f/f}$ *Vav1-icre*$^{+/-}$ (*Tet2*$^{-/-}$) genotypes (exon 3 of *Tet2* gene is floxed) in the hematopoietic system. For infection experiments, mice were transported to the McMaster Central Animal Facility (Hamilton, ON, Canada) and maintained under a 12-h light-dark cycle at 22 ±2°C and 55 ± 5% air humidity. Mice had *ad libitum* access to Teklad irradiated global 14% protein diet (Cat. no. 2914, Envigo) and autoclaved reverse osmosis water. Any mice that developed tumors during the entire period of observation were omitted from analyses.

Streptococcus pneumoniae infection

8 to 10-month-old male and female mice were intranasally inoculated with 40µL 10^4 CFU of *S. pneumoniae* P1542, serotype 4, as described previously (53). While risk of pneumococcal disease increases with age, were unable to use aged mice (> 18 months) due to the increased incidence of tumor formation in *Tet2*$^{-/-}$ mice. Mice were given *ad libitum* access to Ensure and HydroGel and the cages were placed on heating pads for the 10-day duration of the infection (experimental endpoint at 10 days p.i.). Mice were monitored three times daily, and if any mouse became moribund (critical endpoint) or lost 20% body weight, it was immediately sacrificed.

Sample collection and tissue processing

Prior to mouse euthanasia, retro-orbital blood collections were used for immunophenotyping, whole blood stimulations, LeukoSpins, and sera collection. Mice were then exsanguinated, and laparotomies performed. Tissues were immediately collected and fixed in 10% neutral buffered formalin (48 hours, 4 °C [Fisher Cat. No. SF100-4]) for hematoxylin and eosin (H&E) staining and immunohistochemistry. Murine BM progenitors were collected from the vertebral column for immunophenotyping or differentiated into macrophages for functional assays as previously published (54).

Histopathological scoring and immunohistochemistry

The lung histopathology was conducted by two blind observers as previously described (55). The Core Histology Facility at the McMaster Immunology Research Centre performed the lung immunohistochemistry. Briefly, paraffin-embedded tissue sections were dewaxed, hydrated, and treated with Bond ER2 (Leica Cat. No. AR9640) for epitope retrieval. Slides were then stained with anti-F4/80 (Bio-Rad Cat. No. MCA-497R; 1:1000 dilution) or anti-Ly6G (BioLegend Cat. No. 127602; 1:1000 dilution) antibodies using the Leica Bond Rx Automated Stainer and the Bond Polymer Refine detection kit. An external rabbit anti-rat secondary antibody (Vector labs Cat. No. BA-4001), which was preabsorbed against mouse, was then used to visualize the mononuclear phagocytes ($F4/80^+$ macrophages, monocytes, and dendritic cells) and neutrophils ($Ly6G^+$).

Immunophenotyping by flow cytometry

For whole blood and BM immunophenotyping, 100 μL of heparinized blood and isolated BM were incubated with antibodies (Supplemental Table 2) for 30 min at room temperature and then incubated in 1x dilution of 1-step Fix/Lyse buffer (eBioscience, Cat. No. 00-5333-54) for 10 min. Cells were washed and resuspended in fluorescence-activated cell sorting (FACS) wash buffer (PBS, 0.5% bovine serum albumin, 2 mM EDTA) prior to analysis. For intracellular markers, samples were incubated in the presence of 50 ng/ ml LPS or vehicle control for 4 hours. Following incubation, cells were initially surface stained with antibodies and then intracellular staining was performed after 30 min permeabilization at room temperature with 1x Intracellular Staining Permeabilization Wash Buffer (BioLegend Cat. No. 421002) as previously described (24). Absolute cell counts were determined using CountBright^{TM} Absolute Counting Beads (Life Technologies Cat. No. C36950).

Gating strategies for HSC, monocyte, and neutrophil populations are provided in Supplemental Figures 4-6, for humans and mice. All fluorescence gates were set using appropriate isotype controls or FMOs and compensation of spectral overlap was performed for all fluorochromes. Flow cytometry was performed on a Cytoflex (Beckman-Coulter, U.S.A) and analyzed using FlowJo software (version 10.7.1, Becton Dickinson & Company). Data is reported as percent positive or absolute count for each cell subset.

Measurement of cytokine production

Serum IFNγ, IL10, IL1β, IL6, MCP1, and TNF were measuring using high-sensitivity ELISA as per manufacturer's recommendations (Meso Scale Discovery Cat. No. K15069L-1). Lung TNF, IL6, CCL2, and CXCL1 were measured by qPCR as previously reported.

Whole blood bacterial binding and uptake assay

The bacterial binding and uptake assay using whole blood has been described previously (56). Briefly, to visualize *S. pneumoniae* binding and engulfment capacity of phagocytes, TRITC labeled bacteria were incubated with whole blood for 1h at an MOI of 50. Leukocytes were fixed, stained and analyzed by flow cytometry.

BM derived macrophage killing assay

For the macrophage killing assay, $5x10^5$ BM derived macrophages were preincubated with *S. pneumoniae* at a multiplicity of infection (MOI) of 100 bacteria per macrophage for 60 min at 37°C with gentle shaking to allow for phagocytosis. Viable CFUs of surviving bacteria were determine by culturing supernatants on TS agar plates.

Neutrophil phagocytosis and migration assay

BM was isolated from age-sex matched two to four-month old mice as previously described (57), and neutrophil enrichment followed subsequently using the EasySep™ Mouse Neutrophil Enrichment Kit (StemCell Technologies Cat. No. 19762) according to the manufacturer's instructions. The resulting neutrophil sample purity was assessed by a hematopathologist using hematoxylin and eosin staining, and CD11b and Ly6G flow cytometric analysis, confirming expected purity. Neutrophils were stained with Mitotracker Deep Red (ThermoFisher Scientific) and Nuc Blue (ThermoFisher Scientific). $5x10^5$ cells in 0.5mL of phenol red-free RPMI (Gibco) supplemented with 10% pooled mouse serum were plated per 35mm glass bottom imaging dish

(Mattek corporation). GFP-labeled *Staphylococcus aureus* was grown overnight to an OD_{600} of 0.5, and subsequently co-cultured with neutrophils at a ratio of 10:1. Time lapse imaging was performed using the SP8-X confocal scanning microscope (Leica) and four fields of view were captured over 30 min per sample. Phagocytosis, migration and NET surface area were analyzed in FIJI after stitching the four fields of view together. *Staphylococcus aureus* counts per cell were performed. Migration analysis was performed using the TrackMate plugin, and max distance (between farthest two points) of each cell track and average speed along each track were quantified. To determine differences in trans-endothelial migration of circulating leukocytes, we intraperitoneally injected mice with 100 nM MCP-1/CCL2 and measured leukocyte recruitment after 4 hours, as previously reported.(24)

Sequencing of RNA

RNA was extracted from neutrophils as previously described (58). Briefly, RNA was extracted using the RNeasy Mini Kit (Qiagen Cat. No. 74104) following the manufacturer's instructions. Aliquots of RNA were quantified on the Bioanalyzer RNA 6000 Nano kit (Agilent, Santa Clara, CA) and stored at -80 C for qRT-PCR analysis. 120-300ng of RNA was used to generate libraries for two independent RNA-Seq experiments by the QuantSeq 3' mRNA-Seq library prep kit for Illumina (Lexogen, Vienna, Austria). Libraries were generated by 3' poly-A tail capture for quantification of mRNA transcripts. Sequencing was performed on the Illumina NextSeq platform at the QCPU core facility (Single end, 75bp read length, 130 million reads).

Bioinformatic Analysis of RNA-seq data

The raw Fastq files were de-multiplexed and trimmed using Fastp (59). This was followed by alignment of the reads, which was performed on the Queen's Center for Advanced Computing computer cluster. The quality of reads was analyzed using the FastQC module. Alignment of reads was performed by the STAR (Spliced Transcripts Alignment to a Reference (60)) tool and the trimmed fastq files were aligned to the current mouse gene assembly, GRCm38, using the GENCODE VM23 annotation. Normalization of sequence depth, distribution, correlation, batch effects and outliers were then all performed using the DESeq2 analysis program (61). Tables of gene counts were then created. Finally, analysis of gene expression was performed in R using DESeq2 (61). The analysis focused on the differences between *Tet2*$^{f/f}$ versus *Tet2*$^{-/-}$ neutrophils under baseline (no treatment) conditions. This is because we were interested in seeing the changes in neutrophil gene expression and function in the steady state. The lists of significantly upregulated and downregulated genes were then merged to conduct pathway enrichment analysis/genome ontology (GO), which was performed using the g:Profiler (62). Differential expression counts were then visualized through Volcano Plots (Supplemental Figure S7) and normalized counts were graphed using Prism GraphPad. A P-value < 0.05 was considered significant. Students t-tests were used to calculate significance for normalized counts.

Statistical Analysis

Statistical analyses were performed in GraphPad Prism V9.2 or R 4.1.2. For UK Biobank data analysis, Cox Proportional Hazards regression were used to estimate the risk of incident infections by CHIP and *TET2* status. Covariables of age, age^2, sex, smoking history, and 10 principal components of genetic ancestry were added to the model. In a separate model, we added an interaction term from a common SNP in the IL6 receptor that is associated with lower IL6 signaling

(rs2228415). For the animal models, the data were tested for normality using Shapiro-Wilk test, and a one-way analysis of variance (ANOVA) was used to compare mean differences amongst groups with Benjamini-Hochberg multiple testing correction applied as needed. For comparisons between two groups, significance was calculated using a 1-tailed Student's t-test or Mann-Whitney test where appropriate. The results are expressed as the mean value with standard error of the mean (SEM), unless otherwise stated. Significance levels used are $*P<0.05$, $**P<0.01$, $***P<0.001$. Genes and GO terms are reported for adjusted p-values and FDR values <0.05.

DATA AVAILABILITY

Datasets supporting the results of this article are available in the Open Science Framework (OSF) database repository at https://osf.io/bcta2/.

STUDY APPROVAL

The animal ethics have been approved by the McMaster Animal Research Ethics Board (no. 17-05-19) and Queen's University Animal Care committee (Protocol 2021-2128) and performed in accordance with the Canadian Council on Animal Care guidelines. All human protocols were approved by the Hamilton Research Ethics Board (#4640) and Queen's University Health Sciences and Affiliated Teaching Hospitals (HSREB) (PATH-181-18). Informed consent was received prior to participation.

AUTHOR CONTRIBUTIONS

DMEB and MJR conceived and funded the experiments. DMEB, MJR, and CQ designed the experiments. CQ, END, AEK, and JAB performed flow cytometry. KZ performed qPCR and assisted with functional assays. CQ and END performed animal experiments and tissue collection. CV, MB and AB performed UK Biobank data analyses. EKC, YZL, SS, AJM, JM, KDS, CH and SLA performed and supported murine neutrophil functional and transcriptomic studies at Queen's. CQ performed IF, histological evaluation and critically evaluated all the data. CQ and AEK performed LeukoSpin analysis. CQ, MR and DMEB wrote the paper. All co-authors edited the paper.

ACNOWLEDGMENTS

We thank Clare A. Edwards for technical assistance and Catherine M. Andary for being a second scorer for IF and histopathological analysis. We also thank Drs. Elsa N. Bou Ghanem and Manmeet Bhalla for their assistance with the neutrophil killing assays. DMEB was funded through the Canadian Research Chairs program and CIHR. CQ was supported by a CIHR Postdoctoral Fellowship Award. JB was supported by a MIRA fellowship. This study was supported by a project grant from the CIHR (PJT-156291).

CONFLICT OF INTEREST

All authors declared no conflict of interest.

REFERENCES

1. Groarke EM, and Young NS. Aging and Hematopoiesis. *Clin Geriatr Med.* 2019;35(3):285-93.
2. Cooper JN, and Young NS. Clonality in context: hematopoietic clones in their marrow environment. *Blood.* 2017;130(22):2363-72.
3. Steensma DP, Bejar R, Jaiswal S, Lindsley RC, Sekeres MA, Hasserjian RP, et al. Clonal hematopoiesis of indeterminate potential and its distinction from myelodysplastic syndromes. *Blood.* 2015;126(1):9-16.
4. Vlasschaert C, McNaughton AJM, Chong M, Cook EK, Hopman W, Kestenbaum B, et al. Association of Clonal Hematopoiesis of Indeterminate Potential with Worse Kidney Function and Anemia in Two Cohorts of Patients with Advanced Chronic Kidney Disease. *J Am Soc Nephrol.* 2022;33(5):985-95.
5. Jaiswal S, and Ebert BL. Clonal hematopoiesis in human aging and disease. *Science.* 2019;366(6465).
6. Steensma DP. Clinical consequences of clonal hematopoiesis of indeterminate potential. *Blood Adv.* 2018;2(22):3404-10.
7. Zhang X, Su J, Jeong M, Ko M, Huang Y, Park HJ, et al. DNMT3A and TET2 compete and cooperate to repress lineage-specific transcription factors in hematopoietic stem cells. *Nat Genet.* 2016;48(9):1014-23.
8. Moran-Crusio K, Reavie L, Shih A, Abdel-Wahab O, Ndiaye-Lobry D, Lobry C, et al. Tet2 loss leads to increased hematopoietic stem cell self-renewal and myeloid transformation. *Cancer Cell.* 2011;20(1):11-24.
9. Ko M, Bandukwala HS, An J, Lamperti ED, Thompson EC, Hastie R, et al. Ten-Eleven-Translocation 2 (TET2) negatively regulates homeostasis and differentiation of hematopoietic stem cells in mice. *Proc Natl Acad Sci U S A.* 2011;108(35):14566-71.
10. Li Z, Cai X, Cai CL, Wang J, Zhang W, Petersen BE, et al. Deletion of Tet2 in mice leads to dysregulated hematopoietic stem cells and subsequent development of myeloid malignancies. *Blood.* 2011;118(17):4509-18.
11. Cole CB, Russler-Germain DA, Ketkar S, Verdoni AM, Smith AM, Bangert CV, et al. Haploinsufficiency for DNA methyltransferase 3A predisposes hematopoietic cells to myeloid malignancies. *J Clin Invest.* 2017;127(10):3657-74.
12. Lim GB. Clonal haematopoiesis induces a pro-inflammatory monocyte phenotype in HF. *Nat Rev Cariol.* 2021;18(74).
13. Abplanalp WT, Cremer S, John D, Hoffmann J, Schuhmacher B, Merten M, et al. Clonal Hematopoiesis-Driver DNMT3A Mutations Alter Immune Cells in Heart Failure. *Circ Res.* 2021;128(2):216-28.
14. Jaiswal S, Natarajan P, Silver AJ, Gibson CJ, Bick AG, Shvartz E, et al. Clonal Hematopoiesis and Risk of Atherosclerotic Cardiovascular Disease. *N Engl J Med.* 2017;377(2):111-21.
15. Fuster JJ, MacLauchlan S, Zuriaga MA, Polackal MN, Ostriker AC, Chakraborty R, et al. Clonal hematopoiesis associated with TET2 deficiency accelerates atherosclerosis development in mice. *Science.* 2017;355(6327):842-7.
16. Cai Z, Kotzin JJ, Ramdas B, Chen S, Nelanuthala S, Palam LR, et al. Inhibition of Inflammatory Signaling in Tet2 Mutant Preleukemic Cells Mitigates Stress-Induced Abnormalities and Clonal Hematopoiesis. *Cell Stem Cell.* 2018;23(6):833-49 e5.
17. Ferrone CK, Blydt-Hansen M, and Rauh MJ. Age-Associated TET2 Mutations: Common Drivers of Myeloid Dysfunction, Cancer and Cardiovascular Disease. *Int J Mol Sci.* 2020;21(2).

18. Luskin MR, Cronin, A.M., Copson, K., Jung, W., Wadleigh, M., DeAngelo, M.J., Steensma, D.P., Driver, J., Lane, A.A., Lindsley, C., Abel, G.A. Spliceosome Mutations are Associated with Frailty in Older Patients with Myeloid Malignancies. *Blood.* 2017;130(Supplement 1).
19. Potus F, Pauciulo MW, Cook EK, Zhu N, Hsieh A, Welch CL, et al. Novel Mutations and Decreased Expression of the Epigenetic Regulator TET2 in Pulmonary Arterial Hypertension. *Circulation.* 2020;141(24):1986-2000.
20. Bolton KL, Koh Y, Foote MB, Im H, Jee J, Sun CH, et al. Clonal hematopoiesis is associated with risk of severe Covid-19. *Nat Commun.* 2021;12(1):5975.
21. Murdoch DR, and Howie SRC. The global burden of lower respiratory infections: making progress, but we need to do better. *Lancet Infect Dis.* 2018;18(11):1162-3.
22. Iwai-Saito K, Shobugawa Y, Aida J, and Kondo K. Frailty is associated with susceptibility and severity of pneumonia in older adults (A JAGES multilevel cross-sectional study). *Sci Rep.* 2021;11(1):7966.
23. Kovtonyuk LV, Fritsch K, Feng X, Manz MG, and Takizawa H. Inflamm-Aging of Hematopoiesis, Hematopoietic Stem Cells, and the Bone Marrow Microenvironment. *Front Immunol.* 2016;7:502.
24. Puchta A, Naidoo A, Verschoor CP, Loukov D, Thevaranjan N, Mandur TS, et al. TNF Drives Monocyte Dysfunction with Age and Results in Impaired Anti-pneumococcal Immunity. *PLoS Pathog.* 2016;12(1):e1005368.
25. Kratofil RM, Kubes P, and Deniset JF. Monocyte Conversion During Inflammation and Injury. *Arterioscler Thromb Vasc Biol.* 2017;37(1):35-42.
26. Kimball A, Schaller M, Joshi A, Davis FM, denDekker A, Boniakowski A, et al. Ly6C(Hi) Blood Monocyte/Macrophage Drive Chronic Inflammation and Impair Wound Healing in Diabetes Mellitus. *Arterioscler Thromb Vasc Biol.* 2018;38(5):1102-14.
27. Franceschi C, and Campisi J. Chronic inflammation (inflammaging) and its potential contribution to age-associated diseases. *J Gerontol A Biol Sci Med Sci.* 2014;69 Suppl 1:S4-9.
28. Franceschi C, Bonafe M, Valensin S, Olivieri F, De Luca M, Ottaviani E, et al. Inflamm-aging. An evolutionary perspective on immunosenescence. *Ann N Y Acad Sci.* 2000;908:244-54.
29. Jaiswal S, and Libby P. Clonal haematopoiesis: connecting ageing and inflammation in cardiovascular disease. *Nat Rev Cardiol.* 2020;17(3):137-44.
30. Cobo I, Tanaka T, Glass CK, and Yeang C. Clonal hematopoiesis driven by DNMT3A and TET2 mutations: role in monocyte and macrophage biology and atherosclerotic cardiovascular disease. *Curr Opin Hematol.* 2022;29(1):1-7.
31. Bick AG, Pirruccello JP, Griffin GK, Gupta N, Gabriel S, Saleheen D, et al. Genetic Interleukin 6 Signaling Deficiency Attenuates Cardiovascular Risk in Clonal Hematopoiesis. *Circulation.* 2020;141(2):124-31.
32. Blot M, Croisier D, Pechinot A, Vagner A, Putot A, Fillion A, et al. A leukocyte score to improve clinical outcome predictions in bacteremic pneumococcal pneumonia in adults. *Open Forum Infect Dis.* 2014;1(2):ofu075.
33. Cook EK, Izukawa T, Young S, Rosen G, Jamali M, Zhang L, et al. Comorbid and inflammatory characteristics of genetic subtypes of clonal hematopoiesis. *Blood Adv.* 2019;3(16):2482-6.
34. Geissmann F, Jung S, and Littman DR. Blood monocytes consist of two principal subsets with distinct migratory properties. *Immunity.* 2003;19(1):71-82.
35. Gordon S, and Taylor PR. Monocyte and macrophage heterogeneity. *Nat Rev Immunol.* 2005;5(12):953-64.
36. Serbina NV, and Pamer EG. Monocyte emigration from bone marrow during bacterial infection requires signals mediated by chemokine receptor CCR2. *Nat Immunol.* 2006;7(3):311-7.

37. Abegunde SO, and Rauh MJ. Tet2-Deficient Bone Marrow Progenitors Have a Proliferative Advantage in the Presence of TNF-Alpha and IFN-Gamma: Implications for Clonal Dominance in Inflammaging and MDS. *Blood.* 2015;126(23):2850.
38. Hotchkiss RS, Moldawer LL, Opal SM, Reinhart K, Turnbull IR, and Vincent JL. Sepsis and septic shock. *Nat Rev Dis Primers.* 2016;2:16045.
39. Shen X, Cao K, Zhao Y, and Du J. Targeting Neutrophils in Sepsis: From Mechanism to Translation. *Front Pharmacol.* 2021;12:644270.
40. SanMiguel JM, Eudy E, Loberg MA, Young KA, Mistry JJ, Mujica KD, et al. Distinct Tumor Necrosis Factor Alpha Receptors Dictate Stem Cell Fitness versus Lineage Output in Dnmt3a-Mutant Clonal Hematopoiesis. *Cancer Discov.* 2022;12(12):2763-73.
41. Yeaton A, Cayanan G, Loghavi S, Dolgalev I, Leddin EM, Loo CE, et al. The Impact of Inflammation-Induced Tumor Plasticity during Myeloid Transformation. *Cancer Discov.* 2022;12(10):2392-413.
42. Pechous RD. With Friends Like These: The Complex Role of Neutrophils in the Progression of Severe Pneumonia. *Front Cell Infect Microbiol.* 2017;7:160.
43. Bou Ghanem EN, Clark S, Roggensack SE, McIver SR, Alcaide P, Haydon PG, et al. Extracellular Adenosine Protects against Streptococcus pneumoniae Lung Infection by Regulating Pulmonary Neutrophil Recruitment. *PLoS Pathog.* 2015;11(8):e1005126.
44. Zhang X, Majlessi L, Deriaud E, Leclerc C, and Lo-Man R. Coactivation of Syk kinase and MyD88 adaptor protein pathways by bacteria promotes regulatory properties of neutrophils. *Immunity.* 2009;31(5):761-71.
45. Kulkarni U, Zemans RL, Smith CA, Wood SC, Deng JC, and Goldstein DR. Excessive neutrophil levels in the lung underlie the age-associated increase in influenza mortality. *Mucosal Immunol.* 2019;12(2):545-54.
46. Sawant KV, Poluri KM, Dutta AK, Sepuru KM, Troshkina A, Garofalo RP, et al. Chemokine CXCL1 mediated neutrophil recruitment: Role of glycosaminoglycan interactions. *Sci Rep.* 2016;6:33123.
47. Capucetti A, Albano F, and Bonecchi R. Multiple Roles for Chemokines in Neutrophil Biology. *Front Immunol.* 2020;11:1259.
48. Jeyaseelan S, Manzer R, Young SK, Yamamoto M, Akira S, Mason RJ, et al. Induction of CXCL5 during inflammation in the rodent lung involves activation of alveolar epithelium. *Am J Respir Cell Mol Biol.* 2005;32(6):531-9.
49. Danikas DD, Karakantza M, Theodorou GL, Sakellaropoulos GC, and Gogos CA. Prognostic value of phagocytic activity of neutrophils and monocytes in sepsis. Correlation to CD64 and CD14 antigen expression. *Clin Exp Immunol.* 2008;154(1):87-97.
50. Hortova-Kohoutkova M, Tidu F, De Zuani M, Sramek V, Helan M, and Fric J. Phagocytosis-Inflammation Crosstalk in Sepsis: New Avenues for Therapeutic Intervention. *Shock.* 2020;54(5):606-14.
51. Vlasschaert C, Mack T, Heimlich JB, Niroula A, Uddin MM, Weinstock JS, et al. A practical approach to curate clonal hematopoiesis of indeterminate potential in human genetic datasets. *Blood.* 2023.
52. Kennedy AE, Cook L, Breznik JA, Cowbrough B, Wallace JG, Huynh A, et al. Lasting Changes to Circulating Leukocytes in People with Mild SARS-CoV-2 Infections. *Viruses.* 2021;13(11).
53. Shen P, Whelan FJ, Schenck LP, McGrath JJC, Vanderstocken G, Bowdish DME, et al. Streptococcus pneumoniae Colonization Is Required To Alter the Nasal Microbiota in Cigarette Smoke-Exposed Mice. *Infect Immun.* 2017;85(10).
54. Thevaranjan N, Puchta A, Schulz C, Naidoo A, Szamosi JC, Verschoor CP, et al. Age-Associated Microbial Dysbiosis Promotes Intestinal Permeability, Systemic Inflammation, and Macrophage Dysfunction. *Cell Host Microbe.* 2017;21(4):455-66 e4.

55. Bergstrom KS, Kissoon-Singh V, Gibson DL, Ma C, Montero M, Sham HP, et al. Muc2 protects against lethal infectious colitis by disassociating pathogenic and commensal bacteria from the colonic mucosa. *PLoS Pathog.* 2010;6(5):e1000902.
56. Novakowski KE, Loukov D, Chawla V, and Bowdish DM. Bacterial Binding, Phagocytosis, and Killing: Measurements Using Colony Forming Units. *Methods Mol Biol.* 2017;1519:297-309.
57. Amend SR, Valkenburg KC, and Pienta KJ. Murine Hind Limb Long Bone Dissection and Bone Marrow Isolation. *J Vis Exp.* 2016(110).
58. Luo M. *Pathology and Molecular Medicine*. QSpace: Queens University; 2020.
59. Chen S, Zhou Y, Chen Y, and Gu J. fastp: an ultra-fast all-in-one FASTQ preprocessor. *Bioinformatics.* 2018;34(17):i884-i90.
60. Dobin A, Davis CA, Schlesinger F, Drenkow J, Zaleski C, Jha S, et al. STAR: ultrafast universal RNA-seq aligner. *Bioinformatics.* 2013;29(1):15-21.
61. Love MI, Huber W, and Anders S. Moderated estimation of fold change and dispersion for RNA-seq data with DESeq2. *Genome Biol.* 2014;15(12):550.
62. Raudvere U, Kolberg L, Kuzmin I, Arak T, Adler P, Peterson H, et al. g:Profiler: a web server for functional enrichment analysis and conversions of gene lists (2019 update). *Nucleic Acids Res.* 2019;47(W1):W191-W8.

FIGURES

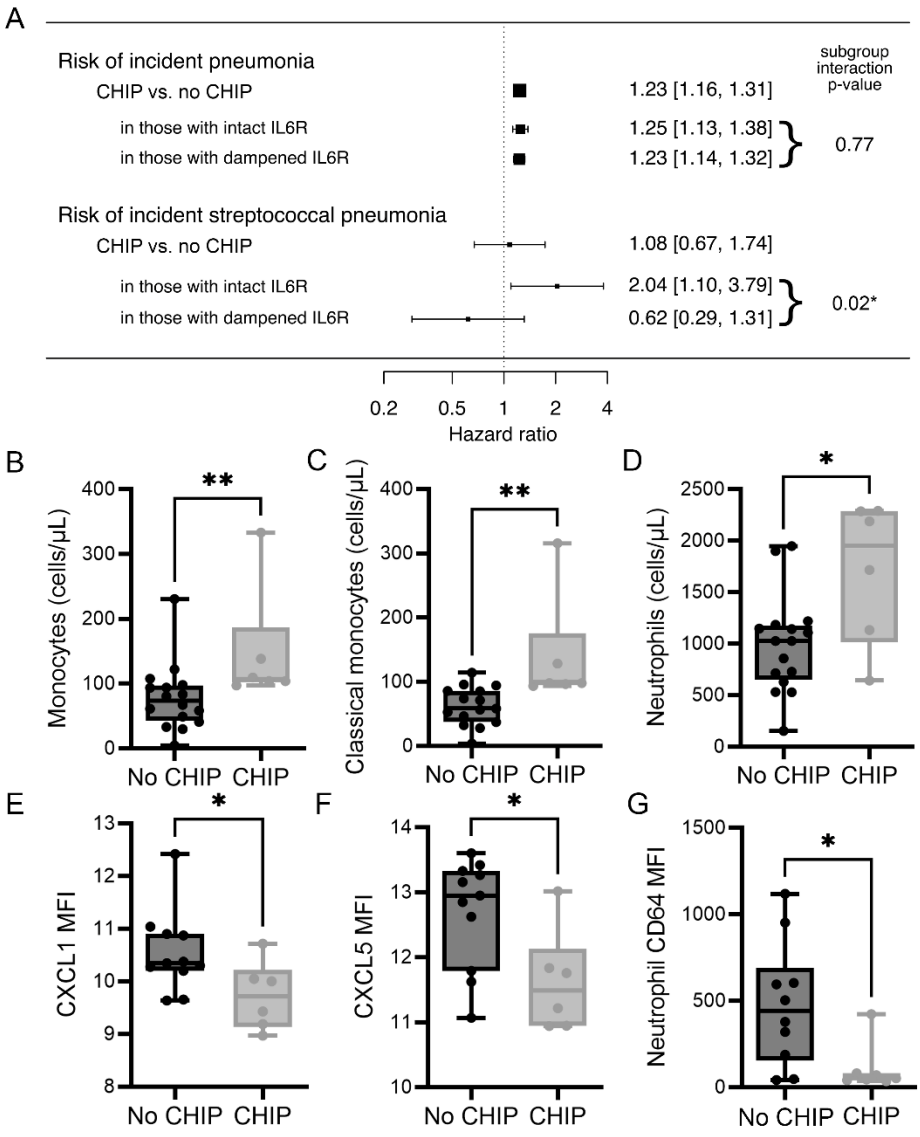

Figure 1. CHIP is positively associated with incident pneumonia including confirmed *Streptococcus pneumoniae* pneumonia (A) CHIP is positively associated with incident all-cause pneumonia among 438,421 individuals in the UK Biobank without a history of pneumonia in a Cox proportional hazards regression model adjusted for age, age^2, sex, smoking history, history of chronic inflammatory lung disease (COPD), and 10 principal components of genetic ancestry. In a model adding an interaction term for a common SNP in the IL6 receptor associated with lower IL6 signaling (rs2228415), CHIP is associated with incident confirmed *S. pneumoniae* pneumonia. The CHIP × rs2228415 interaction term is significantly below 0, suggesting that lower IL6R signaling mitigates the effects of CHIP on pneumonia risk. (B-G) Leukocyte populations were quantified in whole blood from CHIP carriers and non-carriers in a local cohort using flow cytometry. Compared with non-carriers, the numbers of peripheral blood **(B)** monocytes (No CHIP [78.4 ± 12.9]; CHIP [147.6 ± 37.5]), **(C)** classical monocytes (No CHIP [62.4 ± 7.7]; CHIP [138.3 ± 35.9]), and **(D)** neutrophils (No CHIP [990 ± 117]; CHIP [1709 ± 281]), were increased in CHIP carriers.

Chemokines **(E)** CXCL1 (No CHIP [10.5 ± 0.23]; CHIP [9.7 ± 0.26]), and **(F)** CXCL5 (No CHIP [12.7 ± 0.25]; CHIP [11.6 ± 0.32]), were decreased in the sera of CHIP carriers. **(G)** Surface expression of CD64 was decreased on circulating blood neutrophils in CHIP carriers (No CHIP [474.9 ± 113.5]; CHIP [106.6 ± 53.0]). Data are presented as box and whisker plots, minimum to maximum, where the center line represents the median and each dot is a participant. Sample size: 16 No CHIP, 6 CHIP participants. Significant outliers removed using ROUT method. MFI – Geometric Mean Fluorescence Intensity. Significance was assessed by Mann-Whitney test. $*P \leq 0.05$, $**P \leq 0.01$, $***P \leq 0.001$

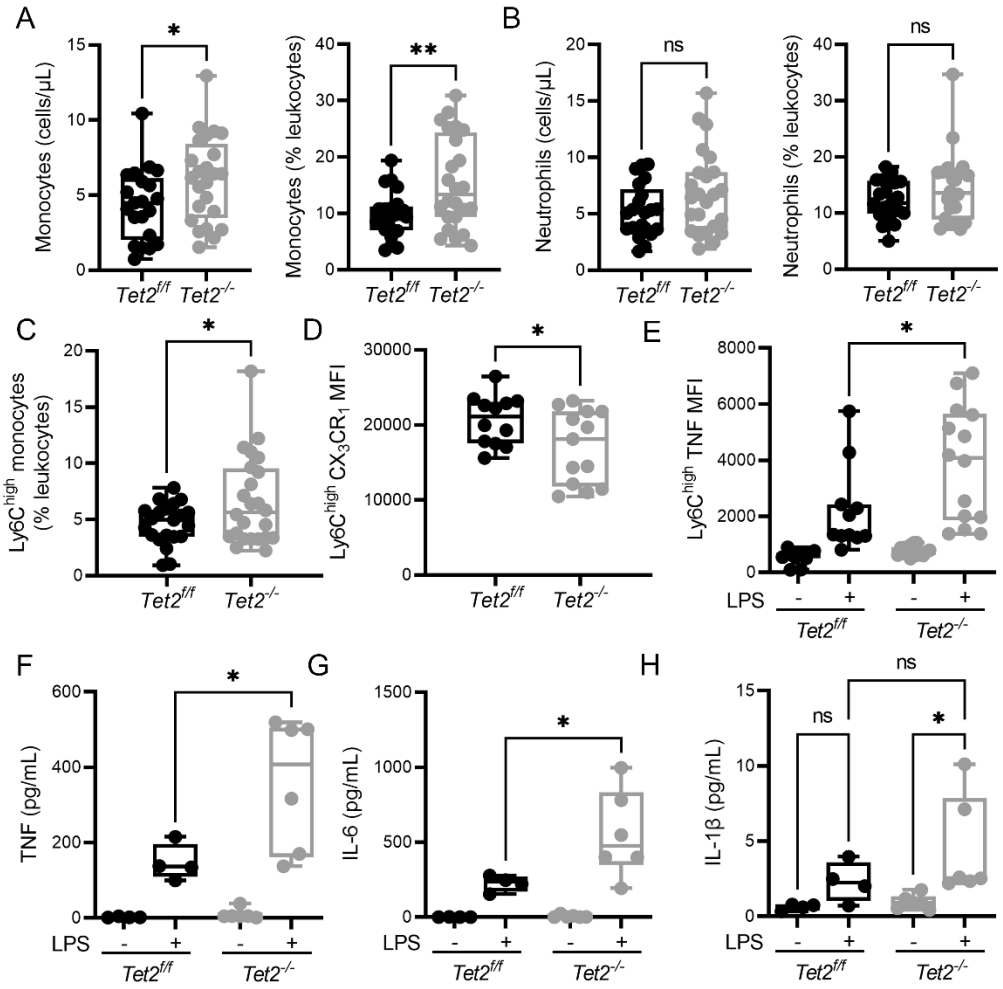

Figure 2. Expansion of inflammatory monocytes in peripheral blood following *TET2* loss. (A) Flow cytometric analysis of peripheral blood revealed an increase in the number (*Tet2*$^{f/f}$ [111 ± 13.07], n=21; *Tet2*$^{-/-}$ [157.5 ± 15], n=24) and proportion (*Tet2*$^{f/f}$ [9.85 ± 0.89]; *Tet2*$^{-/-}$ [15.43 ± 1.66]) of monocytes in *Tet2*$^{-/-}$ mice. **(B)** There was a tendency towards increase in the number (*Tet2*$^{f/f}$ [135 ± 12.7], n=21; *Tet2*$^{-/-}$ [177.4 ± 18.58], n=24) and relative proportion (*Tet2*$^{f/f}$ [12.3 ± 0.78]; *Tet2*$^{-/-}$ [14.4 ± 1.34]) of circulating neutrophils in *Tet2*$^{-/-}$ mice. **(C)** The proportion of Ly6C^{high} inflammatory monocytes, as a proportion of total CD45^{+} leukocytes, increased in the circulation of *Tet2*$^{-/-}$ mice (6.63 ± 0.81) as compared to *Tet2*$^{f/f}$ mice (4.60 ± 0.39). **(D)** This corresponded with a decrease in the surface expression of CX_3CR_1 (*Tet2*$^{f/f}$ [20657 ± 945.6]; *Tet2*$^{-/-}$ [17057 ± 1355]). **(E)** Intracellular staining of TNF revealed higher TNF expression in the peripheral blood of *Tet2*$^{-/-}$ mice (4050 ± 662) following 4-hour stimulation with LPS, as compared to *Tet2*$^{f/f}$ mice (2202 ± 566.4) **(F)** Results from a multiplex-ELISA showed that whole blood from *Tet2*$^{-/-}$ mice had a significant increase in TNF (*Tet2*$^{f/f}$ [147 ± 24.3]; *Tet2*$^{-/-}$ [357 ± 71.2]) and **(G)** IL6 (*Tet2*$^{f/f}$ [225 ± 26.3]; *Tet2*$^{-/-}$ [553 ± 119]) as compared to *Tet2*$^{f/f}$ mice, following 4hr stimulation with LPS *ex vivo*. **(H)** There was a significant induction of IL1β in whole blood from *Tet2*$^{-/-}$ mice following LPS stimulation (4.48 ± 1.3) that was not observed in blood stimulated from *Tet2*$^{f/f}$ mice (2.3 ± 0.7). Data are presented as box and whisker plots, minimum to maximum, where the center line represents the median and each dot is a mouse. MFI – Geometric Mean Fluorescence Intensity. Significance was assessed by Kruskal-Wallis test. *$P \leq 0.05$, **$P \leq 0.01$, ns = not significant.

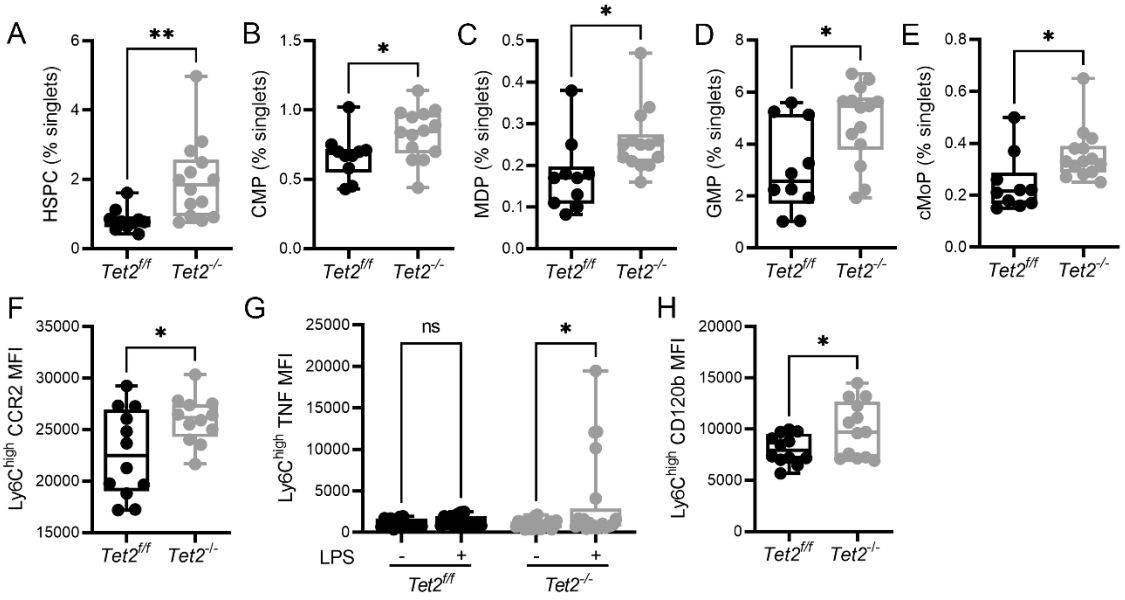

Figure 3. Mutations in *Tet2* increase the proportion of myeloid progenitor cells in the bone marrow. Flow cytometry analysis of the hematopoietic compartment showed an increase in the relative proportion of **(A)** hematopoietic stem and progenitor cells (HSPC) (*Tet2*$^{f/f}$ [0.83 ± 0.10], n=10; *Tet2*$^{-/-}$ [1.95 ± 0.30], n=14), **(B)** common myeloid progenitor (CMP) (*Tet2*$^{f/f}$ [0.66 ± 0.05]; *Tet2*$^{-/-}$ [0.82 ± 0.04]), **(C)** monocyte-dendritic progenitor (MDP) (*Tet2*$^{f/f}$ [0.17 ± 0.02]; *Tet2*$^{-/-}$ [0.25 ± 0.02]), **(D)** granulocyte-monocyte progenitors (GMP) (*Tet2*$^{f/f}$ [3.06 ± 0.54]; *Tet2*$^{-/-}$ [4.82 ± 0.40]), **(E)** and common monocyte progenitors (cMoP) (*Tet2*$^{f/f}$ [0.24 ± 0.03]; *Tet2*$^{-/-}$ [0.35 ± 0.02]) in *Tet2*$^{-/-}$ mice as compared to *Tet2*$^{f/f}$ mice. **(F)** Inflammatory Ly6C^{high} monocytes within the bone marrow of *Tet2*$^{-/-}$ mice had higher expression of the surface C-C chemokine receptor type 2 (CCR2) (*Tet2*$^{f/f}$ [22695 ± 1222]; *Tet2*$^{-/-}$ [25971 ± 656]), as compared to *Tet2*$^{f/f}$ mice. **(G)** These monocytes were hyper-responsive to *ex vivo* stimulation with LPS and had a significant induction of intracellular TNF expression, whereas monocytes from *Tet2*$^{f/f}$ did not. **(H)** Expression of the cell surface TNF receptor, CD120b, was increased on mutant-*TET2* Ly6C^{high} monocytes (*Tet2*$^{f/f}$ [8055 ± 412]; *Tet2*$^{-/-}$ [10013 ± 746]) in the bone marrow. Data are presented as box and whisker plots, minimum to maximum, where the center line represents the median and each dot is a mouse. MFI – Geometric Mean Fluorescence Intensity. Significance was assessed by Mann-Whitney test. *$P \leq 0.05$, **$P \leq 0.01$, ns = not significant.

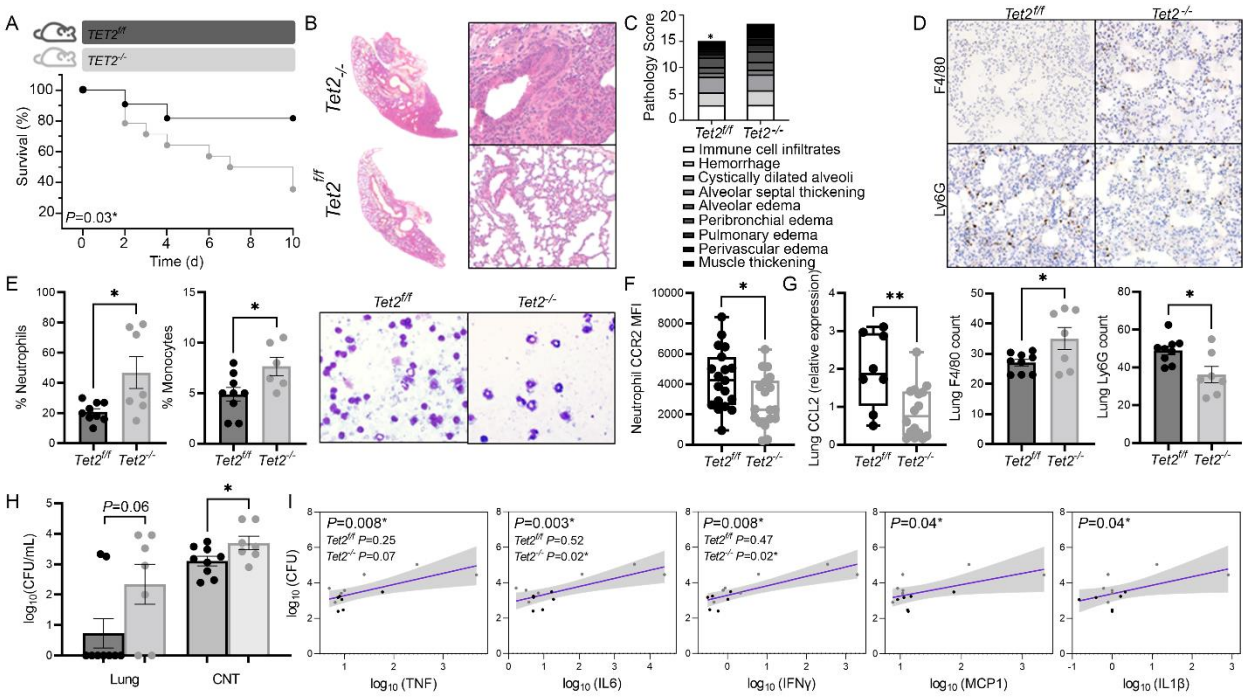

Figure 4. Pneumococcal pneumonia-induced sepsis and accompanying inflammatory responses are exacerbated in Tet2$^{-/-}$ mice. (A) Experimental timeline of infection and concurrent survival (n=13 *Tet2*$^{-/-}$; n=12 *Tet2*$^{f/f}$). **(B)** Representative hematoxylin-and-eosin (H&E)-stained lung sections of mice at 10 days p.i. with *S. pneumoniae*. Magnification 20-fold. **(C)** Histopathological analysis of lung H&E tissue sections [as shown in (B)] attained by two blinded scorers. **(D)** Counts and representative immunohistochemistry staining of mononuclear phagocytes (F4/80^{+}) and neutrophils (Ly6G^{+}) on lung sections at 10 days p.i. Magnification 200-fold. *Tet*$^{-/-}$ mice had increased numbers of mononuclear phagocytes in the lungs (*Tet2*$^{f/f}$ [27 ± 1]; *Tet2*$^{-/-}$ [35 ± 3.6]). In contrast, neutrophils were decreased (*Tet2*$^{f/f}$ [49 ± 2.3]; *Tet2*$^{-/-}$ [36 ± 4.2]). **(E)** Relative frequency, as a percentage of 100 cells counted via LeukoSpins, of neutrophils and monocytes in circulation 10 days p.i. showed an increase in neutrophils (*Tet2*$^{f/f}$ [20.9 ± 2.1]; *Tet2*$^{-/-}$ [46.9 ± 10.5]) and monocytes (*Tet2*$^{f/f}$ [4.9 ± 0.7]; *Tet2*$^{-/-}$ [7.6 ± 2.2]) in *Tet2*$^{-/-}$ mice. Representative images are shown. **(F)** Surface expression of CCR2 is decreased on peripheral blood neutrophils in *Tet2*$^{-/-}$ mice (*Tet2*$^{f/f}$ [4328 ± 449, n=19]; *Tet2*$^{-/-}$ [2875 ± 407], n=18), at steady-state. **(G)** Relative expression of CCL2 is lower in the lungs of *Tet2*$^{-/-}$ at steady-state (*Tet2*$^{f/f}$ [1.96 ± 0.35], n= 8; *Tet2*$^{-/-}$ [0.87 ± 0.17], n=16). **(H)** Enumeration of CFUs in lungs and complete nasal turbinate (CNT) 10 days p.i. showed increased pathogen burden in the CNT of *Tet2*$^{-/-}$ mice (*Tet2*$^{f/f}$ [3.1 ± 0.1]; *Tet2*$^{-/-}$ [3.6 ± 0.22]). **(I)** Results from a simple linear regression between CFUs in the CNT at 10 days p.i. and whole blood inflammatory mediators showed a positive association between inflammation and pathogen burden, with a greater relationship in *Tet2*$^{-/-}$ mice. Shaded area represents 95% confidence intervals. * $P < 0.05$

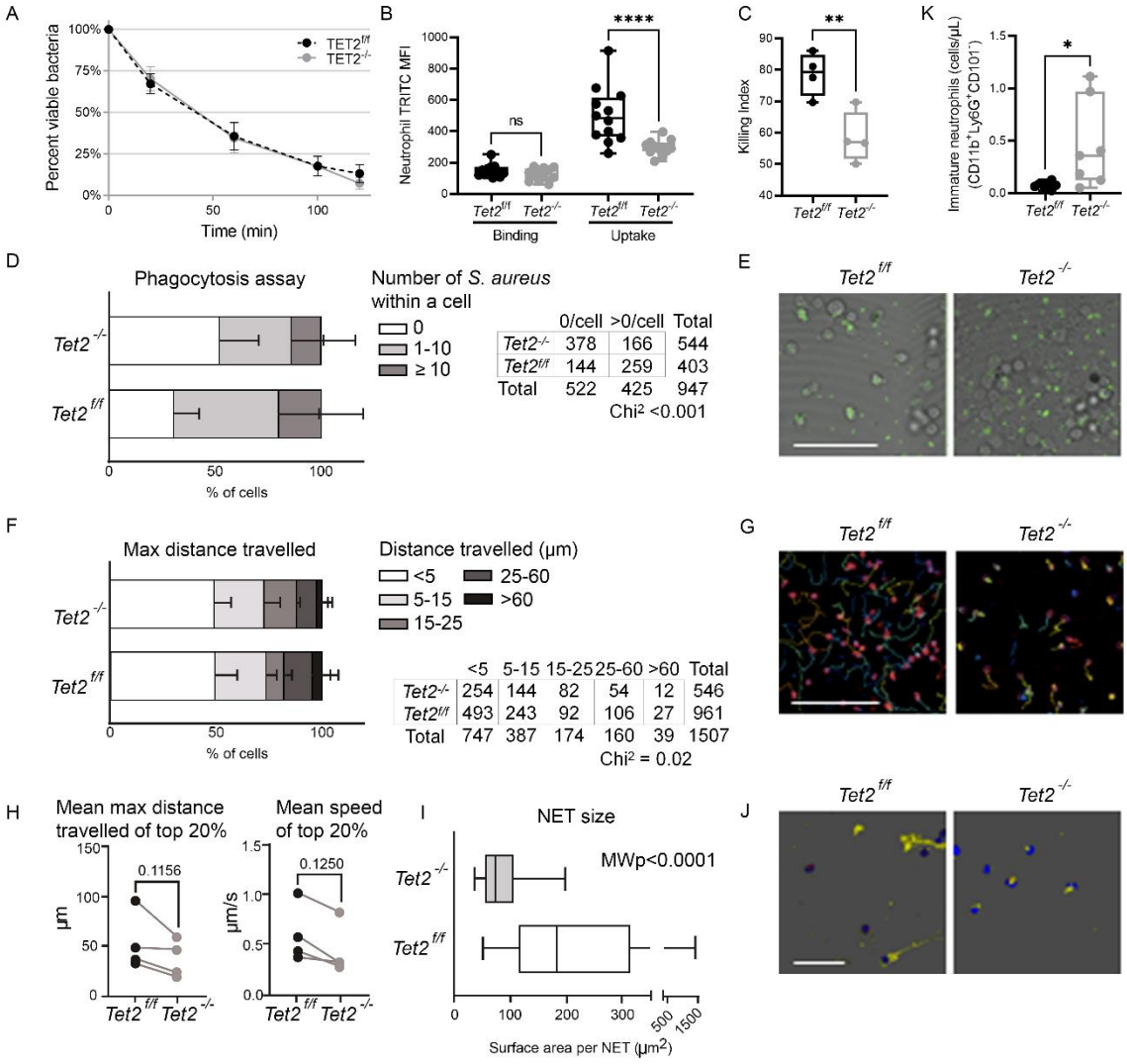

Figure 5. Loss of *Tet2* impairs bactericidal capacity of neutrophils (A) There were no differences in bacterial killing between *Tet2*$^{f/f}$ and *Tet2*$^{-/-}$ BM-derived macrophages. **(B)** Bacterial binding and uptake, measured with pHrodo-Red-labeled *Streptococcus pneumoniae*, showed decreased pathogen uptake in *Tet2*$^{-/-}$ neutrophils (*Tet2*$^{f/f}$ [500 ± 14.6]; *Tet2*$^{-/-}$ [296 ± 14.1]) as compared with *Tet2*$^{f/f}$ neutrophils. **(C)** Intracellular killing of engulfed *S. pneumoniae* was reduced in *Tet2*$^{-/-}$ neutrophils (*Tet2*$^{f/f}$ [78.5 ± 3.5]; *Tet2*$^{-/-}$ [58.3 ± 4.1]). **(D-J)** Functional assays comparing *Tet2*$^{f/f}$ vs. *Tet2*$^{-/-}$ neutrophils over 30 min co-culture with *Staphylococcus aureus*. N=4 independent experiments, each. **(D)** Phagocytosis of *S. aureus* was impaired in *Tet2*$^{-/-}$ neutrophils compared to *Tet2*$^{f/f}$ neutrophils. Means ± SD of percentages of cells with certain counts of internalized bacteria. Significance tested with Chi^2 test. **(E)** Representative image showing GFP-labeled bacteria (green) at end of 30 min co-incubation with neutrophils. Scale bar = 100 µm. **(F-H)** Migration qualities of *Tet2*$^{-/-}$ neutrophils in response to *S. aureus* were impaired compared to *Tet2*$^{f/f}$ neutrophils. **(F)** Means ± SD of percentages of cells travelling certain max distances. Significance tested with Chi^2 test. **(G)** Representative tracks of cells over 30 min co-incubation with *S. aureus*. Scale bar =100 µm. **(H)** Mean max distances travelled (left) and mean speeds of top 20% of cells (right). Significance tested with paired t-test and Wilcoxon, respectively. **(I)** Neutrophil extracellular traps (NETs) were less expansive in *Tet2*$^{-/-}$ (72 µm^2 [54-106]) vs. *Tet2*$^{f/f}$ neutrophils (183 µm^2 [115-312]). Boxes represent median [IQR] of individual NETs

quantified, with min to max whiskers; Mann-Whitney test. **(J)** Representative image of NETs stained for dsDNA (Alexa568, yellow), nuclear DNA, (DAPI, blue), mitochondria (MitoTracker, red), *S. aureus* (GFP, green). Scale bar =100 μm. **(K)** Immature neutrophil counts were higher in the circulation of *Tet2*$^{-/-}$ mice (0.45 ± 0.16; N=7) vs. *Tet2*$^{f/f}$ mice (0.07 ± 0.01; N=7).

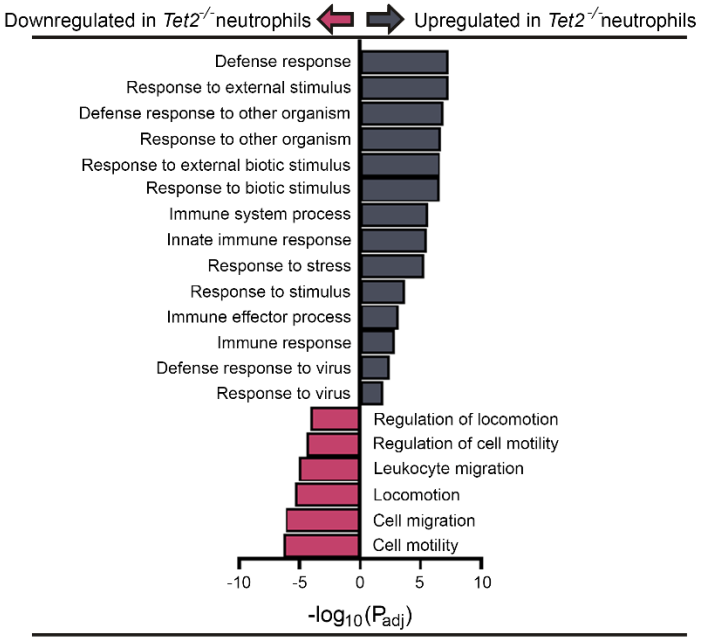

Figure 6. RNA-seq of neutrophils isolated from *Tet2*$^{-/-}$ mice. Gene pathways related to immunity and defense were upregulated in neutrophils isolated from *Tet2*$^{-/-}$ mice, whereas pathways related to motility and locomotion were downregulated.